Crystal structure and elementary properties of Na_xCoO_2 ($x=0.32$, 0.51, 0.6, 0.75, and 0.92) in the three-layer $NaCoO_2$ family

L. Viciu,[1] J. W. G. Bos,[1] H. W. Zandbergen,[2] Q. Huang,[3] M. L. Foo,[1] S. Ishiwata,[1,4] A. P. Ramirez,[5] M. Lee,[6] N. P. Ong,[6] and R. J. Cava[1]

[1]*Department of Chemistry, Princeton University, Princeton, New Jersey 08540, USA*

[2]*National Centre for HREM, Department of Nanoscience, Delft Institute of Technology, Al Delft, The Netherlands*

[3]*NIST Center for Neutron Research, NIST, Gaithersburg, Maryland 20899, USA*

[4]*Department of Applied Physics, Waseda University, Ookubo, Shinjuku, Tokyo, 169-8555, Japan*

[5]*Bell Laboratories, Lucent Technologies, Murray Hill, New Jersey 07974, USA*

[6]*Department of Physics, Princeton University, Princeton, New Jersey 08540, USA*

(Received 25 January 2006; published 2 May 2006)

The crystal structures of Na_xCoO_2 phases based on three-layer $NaCoO_2$, with $x=0.32$, 0.51, 0.60, 0.75, and 0.92, determined by powder neutron diffraction, are reported. The structures have triangular CoO_2 layers interleaved by sodium ions, and evolve with variation in Na content in a more complex way than has been observed in the two-layer Na_xCoO_2 system. The phases with highest and lowest Na content studied ($x=0.92$ and 0.32) are trigonal, with three CoO_2 layers per cell and octahedral Na ion coordination. The intermediate compositions have monoclinic structures. The $x=0.75$ compound has one CoO_2 layer per cell, with Na in octahedral coordination and an incommensurate superlattice. The $x=0.6$ and 0.51 phases are also single layer, but the Na is found in trigonal prismatic coordination. The magnetic behavior of the phases is similar to that observed in the two-layer system. Both the susceptibility and the electronic contribution to the specific heat are largest for $x=0.6$.

DOI: 10.1103/PhysRevB.73.174104 PACS number(s): 61.12.Ld, 61.66.Fn, 61.50.Nw, 75.40.Cx

I. INTRODUCTION

Na_xCoO_2 has been widely studied as the solid-state cathode in Na batteries.[1] The discovery in 2003 of superconductivity ($T_C=4.5$ K) in two-layer $Na_{0.3}CoO_2$ intercalated with water[2] made the study of the Na_xCoO_2 system an active area of research. The degree of filling of the Na layer controls the charge in the CoO_2 planes, giving rise to different properties as a function of x. The two-layer form of Na_xCoO_2 has been of significant recent interest, as it displays a variety of interesting properties. In addition to the superconductivity in the hydrated phase, a large thermopower (100 μV/K at 300 K) has been found for $x\sim 0.7$,[3] and attributed to the spin entropy carried by strongly correlated electrons hopping on a triangular lattice.[4] A transition to an insulating state takes place in $Na_{0.5}CoO_2$ at low temperatures, which has been attributed to charge ordering.[5]

Four different phases have been previously reported in the thermodynamic Na_xCoO_2 chemical system.[6] In all the phases, sheets of edge-sharing CoO_6 octahedra are interleaved by sodium ions. The stacking sequence of the oxygen layers gives the number of sheets within a unit cell. Either two or three CoO_2 sheets per unit cell are found. Three of the four phases are reported to be three-layer structures, delineated as (1) the α phase for $0.9\leqslant x\leqslant 1$, (2) the α' phase for $x=0.75$, and (3) the β phase for $0.55\leqslant x\leqslant 0.6$. Only one thermodynamic phase has a two-layer structure; it is known as the γ phase, for $x\sim 0.7$. The coordination of sodium ions in these structures is either octahedral or trigonal prismatic.

These four thermodynamically stable phases in the Na_xCoO_2 system can be obtained by classic solid-state reactions. Topochemical methods can be used to tune the sodium composition within these structures. Thus, two-layer $Na_{0.5}CoO_2$ and $Na_{0.3}CoO_2$ have been obtained by chemical deintercalation of the higher-x counterparts.[7] In addition, chemical intercalation can be used to increase the sodium content of the γ phase from $x=0.7$ up to $x=1$.[7] The crystal structure of two-layer Na_xCoO_2 with $0.3\leqslant x\leqslant 1$ has been extensively studied by Rietveld refinement using neutron diffraction data.[7] In the three-layer structure, however, crystallographic studies are reported only for $x=1$ (single crystals),[8] and for $x=0.67$ (polycrystalline powder).[9] At $x=1$ the reported structure is trigonal [$R\bar{3}m$ with $a=2.889(2)$ and $c=15.609(3)$ Å] while at $x=0.67$ the crystal structure is single-layer monoclinic [$C2/m$, with $a=4.9023(4)$, $b=2.8280(2)$, $c=5.7198(6)$ Å and $\beta=105.964°$]. Early on, the powder patterns for $x=0.5$ and 0.6 were indexed with a monoclinic cell but the structure was not determined.[10]

Here we report a structural study, by neutron powder diffraction analysis, of the Na_xCoO_2 phases derived from three-layer $NaCoO_2$, for $x=0.92$, 0.75, 0.60, 0.51, and 0.32. It is found that the crystal structure changes from one sodium composition to another in an unexpected way. For example, $Na_{0.92}CoO_2$ is trigonal, with Na in octahedral coordination. Deintercalation of this compound using Br_2 results in the formation of $Na_{0.3}CoO_2$, which has the same crystal structure. Deintercalation of trigonal $Na_{0.92}CoO_2$ with I_2 forms $Na_{0.5}CoO_2$, which has a monoclinically distorted single-layer structure. $Na_{0.6}CoO_2$ has also a single-layer unit cell and is found to be isostructural with the previously reported $Na_{0.67}CoO_2$.[9] $Na_{0.75}CoO_2$ has a complex crystal structure. An average structure for this phase is reported based on the main reflections in the neutron diffraction data, indexed with a monoclinic cell. Susceptibility and heat capacity measure-

TABLE I. The types of structures found for the Na_xCoO_2 compounds ($0.3<x<1$). The structure types are (distinguished by Na coordination type and the number of layers per unit cell) *P*2, prismatic, two layer; *O*3, octahedral, three layer; *P*1, prismatic, one layer; *O*1, octahedral, one layer.

Refined composition	Space group	Sodium coordination	Structure type
	Two-layer structures		
$Na_{0.34}CoO_2$[a]	$P6_3/mmc$	Trigonal prism	*P*2
$Na_{0.5}CoO_2$[b]	*Pnmm*	Trigonal prism	*P*2
$Na_{0.63}CoO_2$[a]	$P6_3/mmc$	Trigonal prism	*P*2
$Na_{0.71}CoO_2$[a]	$P6_3/mmc$	Trigonal prism	*P*2
$Na_{0.76}CoO_2$[a]	$P6_3/mmc$	Trigonal prism	*P*2
$Na_{0.80}CoO_2$[a]	$P6_3/mmc$	Trigonal prism	*P*2
Na_1CoO_2[a]	$P6_3/mmc$	Trigonal prism	*P*2
	Three-layer derived structures		
$Na_{0.32}CoO_2$[c]	$R\bar{3}m$	Octahedral	*O*3
$Na_{0.5}CoO_2$[c]	$C2/m$	Trigonal prism	*P*1
$Na_{0.6}CoO_2$[c]	$C2/m$	Trigonal prism	*P*1
$Na_{0.67}CoO_2$[d]	$C2/m$	Trigonal prism	*P*1
$Na_{0.75}CoO_2$[c]	$C2/m$	Octahedral	*O*1
$Na_{0.92}CoO_2$[c]	$R\bar{3}m$	Octahedral	*O*3

[a]Data from Ref. 7.
[b]Data from Ref. 14.
[c]This work.
[d]Data from Ref. 9.

ments are also reported for these phases. Although different crystal structures are found for the three-layer as opposed to the two-layer structures (Table I), the basic electronic properties of these materials are similar, supporting the general understanding that the electronic systems, dominated by the in-plane character of the CoO_2 layers, are highly two dimensional in character.

II. EXPERIMENT

Samples of Na_xCoO_2 with $x=0.92$, 0.75, and 0.60 were obtained as previously described.[6] Stoichiometric amounts of Na_2O_2 (Alfa, 93% min) and Co_3O_4 (Alfa, 99.7%) were mixed together in an argon-filled glove box. The powders were then quickly removed from the glove box and placed in a tube furnace to prevent the hydration of sodium peroxide by air exposure. The temperature was slowly (5 °C/min) increased to 550 °C, held constant for 16 h, and then slowly (5 °C/min) cooled to room temperature under flowing oxygen. No sign of contamination with two-layer structure materials was observed for three-layer derived materials synthesized under the employed conditions. Each targeted compound was reproducibly obtained by choosing the appropriate Na:Co stoichiometry.

$Na_{0.5}CoO_2$ and $Na_{0.3}CoO_2$ were synthesized by chemical deintercalation of $Na_{0.92}CoO_2$. $Na_{0.5}CoO_2$ was prepared by mixing $NaCoO_2$ with excess I_2 (10×) dissolved in acetonitrile. After 5 days of stirring, the product was washed with acetonitrile, dried, and stored under argon. Single crystals of $Na_{0.5}CoO_2$ were obtained by chemical deintercalation of $NaCoO_2$ single crystals stirred with H_2O_2 at room temperature for 5 days. $Na_{0.3}CoO_2$ was obtained by mixing $Na_{0.92}CoO_2$ with a molar excess of 40× bromine dissolved in acetonitrile. The reaction time was 5 days, after which the product was washed with acetonitrile and stored under argon. Minimum exposure to atmospheric conditions is required to prevent water intercalation.

All samples were analyzed by powder x-ray diffraction using Cu $K\alpha$ radiation and a diffracted beam monochromator. Neutron diffraction data were collected on each sample at the NIST Center for Neutron Research on the high-resolution powder neutron diffractometer with monochromatic neutrons of wavelength 1.5403 Å produced by a Cu(311) monochromator. Collimators with horizontal divergences of 15′, 20′, and 7′ of arc were used before and after the monochromator and after the sample, respectively. Data were collected in the 2θ range of 3°–168° with a step size of 0.05°. The structural parameters were refined using the program GSAS.[11] The neutron scattering amplitudes used in the refinements were 0.363, 0.253, and 0.581 ($\times 10^{-12}$ cm) for Na, Co, and O, respectively. All sodium contents for the phases were determined by the structure refinements, and were in good agreement with those expected from nominal compositions.

TABLE II. The cell parameters for three-layer derived Na_xCoO_2 ($x=0.92$, 0.6, 0.51, and 0.32).

Compound	Space group	Cell constants (Å)	Volume (Å^3)	Volume/f.u. (Å^3)
$Na_{0.92}CoO_2$	$R\bar{3}m$ (no. 166)	$a=2.88878(5)$ $c=15.5998(3)$	112.740(5)	37.58
$Na_{0.75}CoO_2$	$C2/m$ (no. 12)	$a=4.9020(5)$ $b=2.8723(3)$ $c=5.7789(7)$ $\beta=111.764(7)°$	75.57(1)	37.79
$Na_{0.60}CoO_2$	$C2/m$ (no. 12)	$a=4.9043(2)$ $b=2.8275(1)$ $c=5.7097(3)$ $\beta=106.052(3)°$	76.089(6)	38.05
$Na_{0.51}CoO_2$	$C2/m$ (no. 12)	$a=4.8809(1)$ $b=2.81535(9)$ $c=5.7738(2)$ $\beta=105.546(2)°$	76.439(4)	38.22
$Na_{0.32}CoO_2$	$R\bar{3}m$ (no. 166)	$a=2.81202(7)$ $c=16.732(1)$	114.58(1)	38.18

TABLE III. Crystallographic data for $O3$-type $Na_{0.92}CoO_2$ in the space group $R\bar{3}m$ (no. 166). $\chi^2=1.39$; $wR_p=4.95\%$; $R_p=4.26\%$. (Uiso=isothermal temperature factor; Occ=occupancy.)

Atom	Wyckoff position	x	y	z	Uiso*100	Occ
Co	3*a*	0	0	0	0.43(3)	1
Na	3*b*	0	0	0.5	0.72(4)	0.921(7)
O	6*c*	0	0	0.26976(3)	0.91(1)	1

Electron microscopy analysis was performed with Philips CM300UT electron microscopes having a field emission gun and operated at 300 kV. Electron-transparent areas of specimens were obtained by crushing them slightly under ethanol to form a suspension and then dripping a droplet of this suspension on a carbon-coated holey film on a Cu or Au grid.

The magnetic susceptibilities were measured with a Quantum Design MPMS superconducting quantum interference device system. Zero-field cooled magnetic data were taken between 2 and 300 K in an applied field of 5 kOe. The specific heat samples were prepared by cold-sintering the sample powder with Ag powder. Measurements were made in a commercial cryostat using the relaxation method. A four-probe method using a Quantum Design PPMS system was used to measure the resistivity of the $x=0.5$ phase in the 5–300 K temperature range.[12]

III. RESULTS

The purity of the Na_xCoO_2 compounds was confirmed by x-ray diffraction analysis, while structural investigations were performed by neutron diffraction analysis. Only $Na_{0.92}CoO_2$ and $Na_{0.32}CoO_2$ had powder diffraction patterns that could be indexed with a hexagonal cell. Their neutron powder patterns were indexed within the trigonal space group $R\bar{3}m$ (no. 166), with the cell parameters given in Table II. None of the intermediate sodium compositions maintained the hexagonal structure. The neutron diffraction patterns of $Na_{0.5}CoO_2$ and $Na_{0.6}CoO_2$ were indexed based on centered monoclinic cells in the space group $C2/m$ (no. 12). The cell constants are presented in Table II. The monoclinic cells arise through shifts of the CoO_2 planes of approximately 1 Å relative to each other to accommodate changes in the local Na–O coordination. The shifts are in one direction, parallel to the crystallographic a axis. The x-ray diffraction pattern of $Na_{0.75}CoO_2$ could be well indexed based on a monoclinic cell (space group $C2/m$), but the neutron diffraction pattern showed the presence of relatively strong incommensurate superstructure reflections also seen in electron diffraction (described below). The main reflections of the neutron diffraction pattern fit the cell parameters presented in Table II. In the following, the nomenclature introduced earlier to describe layered structures of this type[13] is employed to most easily distinguish the phases: O and P designations refer to octahedral or prismatic coordination, respectively, of Na in the phase, and the numerical designation 1, 2, or 3 refers to the number of CoO_2 layers in a unit cell repeat. In this system of nomenclature, the two-layer phases commonly studied are $P2$ compounds, whereas the parent compound for the current studies, $NaCoO_2$, has the $O3$ type.

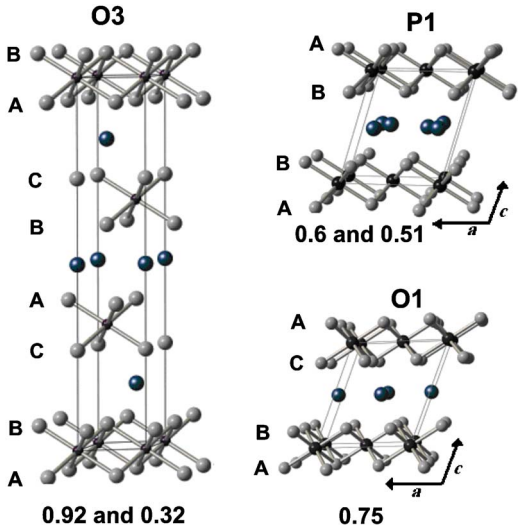

FIG. 1. (Color online) The crystal structures of Na_xCoO_2 phases ($x=0.92, 0.75, 0.6, 0.51, 0.32$) derived from three-layer $NaCoO_2$. Smaller and bigger black spheres represent Co and sodium ions, respectively, while the gray spheres are the oxygen ions.

A. Structural characterization

1. x=0.92 and 0.32 (O3 structure type)

The $Na_{0.92}CoO_2$ and $Na_{0.32}CoO_2$ phases have been found to be isostructural. Their structural analysis by the Rietveld method was carried out in the space group $R\bar{3}m$. The sodium ions are on the $(0, 0, \frac{1}{2})$ site, and are coordinated octahedrally to the oxygens from the CoO_2 layers. The refined structural

TABLE IV. Crystallographic data for $O3$-type $Na_{0.32}CoO_2$ in the space group $R\bar{3}m$ (no. 166). $\chi^2=1.19$; $wR_p=5.26\%$; $R_p=4.33\%$. (Uiso=isothermal temperature factor; Occ=occupancy.)

Atom	Wyckoff position	x	y	z	Uiso*100	Occ
Co	3*a*	0	0	0	0.78(6)	1
Na	3*b*	0	0	0.5	1.2(2)	0.32(1)
O	6*c*	0	0	0.2762(1)	1.07(4)	1

TABLE V. Crystallographic data for $P1$-type $Na_{0.51}CoO_2$ in the space group $C2/m$ (no. 12). $\chi^2=1.48$; $wR_p=4.51\%$; $R_p=3.74\%$. (Uiso=isothermal temperature factor; Occ=occupancy.)

Atom	Wyckoff position	x	y	z	Uiso*100	Occ
Co	2*a*	0	0	0	0.86(5)	1
Na	4*i*	0.806(2)	0	0.491(2)	2.1(2)	0.256(7)
O	4*i*	0.3871(3)	0	0.1740(4)	0.92(3)	1

TABLE VI. Crystallographic data for $P1$-type $Na_{0.6}CoO_2$ in the space group $C2/m$ (no. 12). $\chi^2=2.25$; $wR_p=5.84\%$; $R_p=4.72\%$. (Uiso=isothermal temperature factor; Occ=occupancy.)

Atom	Wyckoff position	x	y	z	Uiso* 100	Occ
Co(1)	2*a*	0	0	0	1.01(5)	1
Na(1)	8*j*	0.812(2)	0.049(6)	0.493(1)	1.6(3)	0.149(3)
O(1)	4*i*	0.3886(2)	0	0.1792(3)	0.94(2)	1

TABLE VII. Crystallographic data for $O1$-type $Na_{0.75}CoO_2$ in the space group $C2/m$ (no. 12). (Uiso=isothermal temperature factor; Occ=occupancy.)

Atom	Wyckoff position	x	y	z	Uiso*100	Occ
Co(1)	2*a*	0	0	0	4.0(2)	1
Na(1)	2*d*	0	0.5	0.5	5.3(3)	0.75
O(1)	4*i*	0.2576(7)	0	0.8179(6)	2.16(8)	1

parameters for both phases are presented in Tables III and IV. Sodium contents of 0.921(7) and 0.32(1) were determined by refinement for these two phases. As an example, the structural model for $Na_{0.92}CoO_2$ is shown in Fig. 1.

2. x=0.6 and 0.51 (P1 structure type)

$Na_{0.6}CoO_2$ and $Na_{0.51}CoO_2$ have similar crystal structures and are found to be isostructural with $Na_{0.67}CoO_2$.[9] This is a single-layer structure (space group $C2/m$) where the sodium ions are in trigonal prismatic coordination. The structural parameters for $Na_{0.6}CoO_2$ and $Na_{0.51}CoO_2$ are presented in Tables V and VI, respectively. Whereas in $Na_{0.51}CoO_2$ the sodium ions are found on the 4*i* site $(x,0,z)$, in $Na_{0.6}CoO_2$ the sodium ions are displaced from the 4*i* site to a more general position 8*j* (x,y,z). No such displacement of the sodium ions was detected for $Na_{0.51}CoO_2$ within the standard deviations of the positional parameters. In these structures, each sodium layer of $Na_{0.51}CoO_2$ has only ~25% of a honeycomb-geometry sodium lattice occupied, while in $Na_{0.6}CoO_2$ the sodium ions form a distorted honeycomb lattice only 30% filled. No information about any possible ordering of the Na ions within the partially occupied sites was obtained in the present study. The peaks observed at $2\theta \sim 24.7°$ and 26.6° in the $Na_{0.51}CoO_2$ neutron powder pattern (see Fig. 2) can be well indexed by doubling the b axis. This suggests that sodium ordering occurs in chains in this structure, much as it does in two-layer $Na_{0.5}CoO_2$.[14,15] No such peaks are observed in the neutron diffraction pattern for three-layer derived $Na_{0.6}CoO_2$. A very good agreement of the sodium content with the nominal compositions is found for both phases by Rietveld refinement: $x=0.596(3)$ and 0.512(4). As an example, the observed and calculated and the difference plots of the refinement for the $x=0.51$ phase are presented in Fig. 2. The idealized crystal structure is shown in Fig. 1.

3. x=0.75 (O1 structure type)

A different crystal structure from the ones described above is found for $Na_{0.75}CoO_2$. The Rietveld refinement was performed in the $C2/m$ space group based on a single-layer structure. The crystal structure of the $x=0.92$ phase was used as a starting model with the atom coordinates in the three-layer structure transformed into the single-layer monoclinic cell. This model gave a very good fit to both the powder x-ray diffraction data ($\chi^2=1.26$, $wR_p=7.86\%$, $R_p=6.22\%$) and the main reflections in the neutron diffraction pattern. The refined structural parameters based on the neutron diffraction data are presented in Table VII. Figure 3 shows the observed and calculated and difference plots for the refinements based on this model for both x-ray data and neutron data (inset in Fig. 3). The structural model is presented in Fig. 1.

Electron diffraction studies were performed to characterize the superstructure observed in the neutron diffraction pattern of $Na_{0.75}CoO_2$. Figure 4 shows a [010] electron diffraction pattern of $Na_{0.75}CoO_2$ taken in nanodiffraction mode

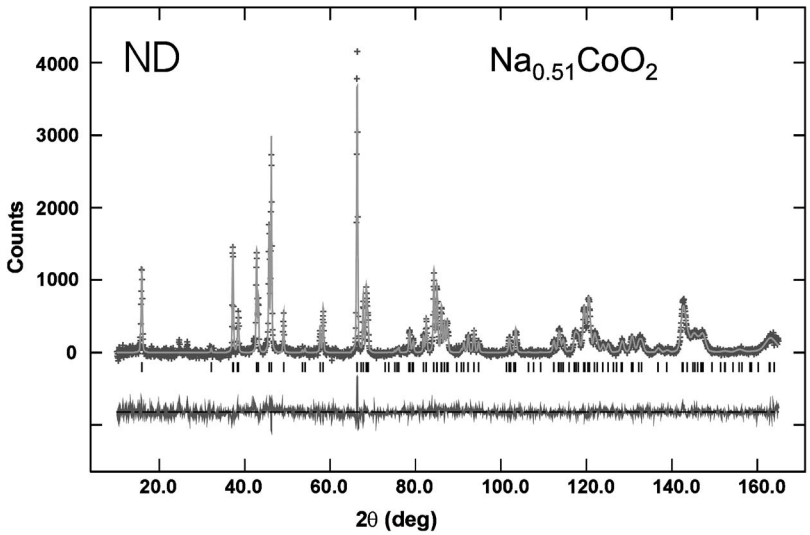

FIG. 2. Observed (crosses) and calculated (solid line) neutron diffraction intensities for $P1$-type $Na_{0.51}CoO_2$ at 295 K. Vertical bars show the Bragg peak positions. The difference plot is shown at the bottom.

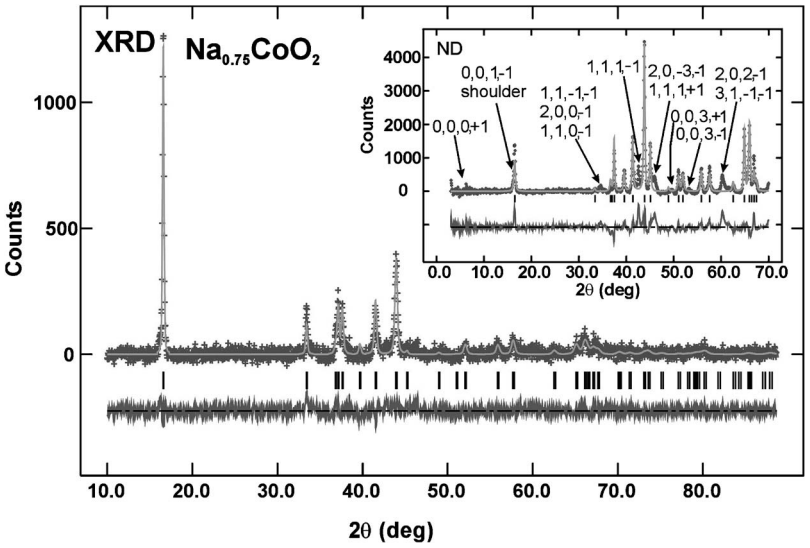

FIG. 3. Observed (crosses) and calculated (solid line) x-ray diffraction intensities for $O1$-type $Na_{0.75}CoO_2$. Vertical bars show the Bragg peak positions. The inset shows the super-reflection peaks (marked with arrows) in the neutron diffraction pattern indexed in a four-dimensional cell.

with a spot size of about 10 nm. A quite dominant superstructure can be distinguished. The superstructure reflections can be indexed best using four dimensions, resulting in four Miller indices *hklm*, in which *m* indicates the order of the satellite measured from the nearby main reflection. The *hklm* indexing of two super-reflections is shown in Fig. 4. The super-reflections in the electron diffraction patterns are much more visible than in the neutron powder diffraction pattern (they are not seen in the x-ray powder pattern). This is due to the strong dynamic scattering in electron diffraction, which results in an enhancement of the weak reflections compared to the strong ones. The observed superstructure for $x=0.75$ is relatively strong, since quite a number of first-order super-reflections can be seen in the neutron diffraction pattern (see Fig. 3). The indexing of the super-reflections in the neutron diffraction pattern is based on the $0.030a^*-0.247c^*$ modulation vector determined from electron diffraction data. Determination of the incommensurately modulated structure of $Na_{0.75}CoO_2$ from the powder diffraction data is beyond the scope of the present study.

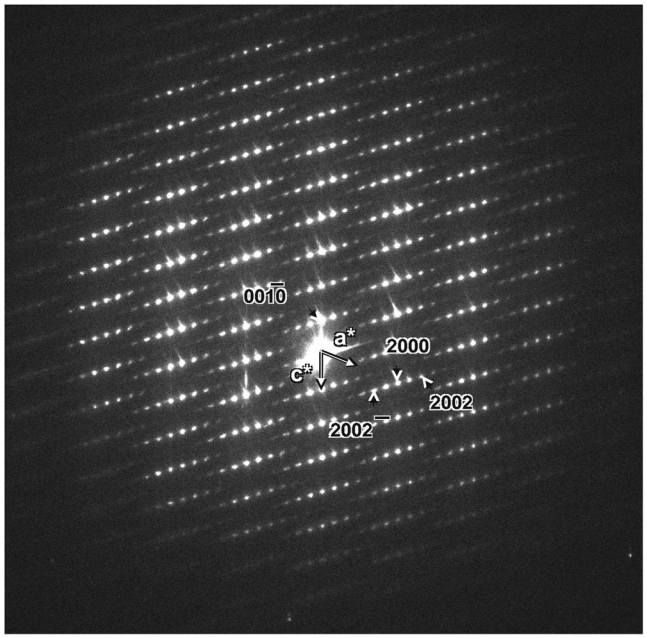

FIG. 4. [010] diffraction pattern of $O1$-type $Na_{0.75}CoO_2$. Strong super-reflections are present. The diffraction pattern was taken with the beam partly on a relatively thick area and partly over the adjacent hole, which configuration resulted in a tail of the reflections to the upper left corner. The indexing of some of the reflections is given. The vector **q** describing the satellites is $0.330\mathbf{a}^*-0.247\mathbf{c}^*$.

B. Magnetic characterization

The variation of molar susceptibility with x is presented in Fig. 5. At temperatures higher than 50 K, the temperature dependence of the susceptibility (χ vs T) for $x \geqslant 0.6$ follows the Curie-Weiss law $\chi=\chi_0+(C/T-\theta)$, with the Curie constant (C), Weiss constant (θ), and temperature independent term (χ_0) presented in Table VIII. The negative Weiss constants indicate antiferromagnetically interacting spins. Given

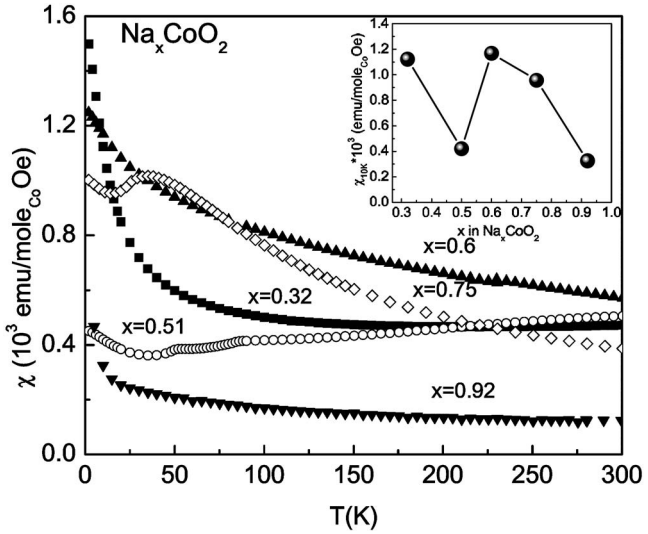

FIG. 5. Temperature dependence of the magnetic susceptibility for three-layer derived Na_xCoO_2 with $x=0.92$, 0.75, 0.6, 0.51, and 0.3.

TABLE VIII. Summary of magnetic data for three-layer derived Na_xCoO_2.

Na_xCoO_2 x	C (cm^3 K/mol)	μ_{eff} (units of μ_B)	θ (K)	χ_0 (emu/mol_{Co} Oe)
0.92	0.0130(5)	0.32	−55(±3)	0.00008(1)
0.75	0.0984(9)	0.88	−48(±1)	0.00011(1)
0.6	0.084(3)	0.82	−97(±3)	0.00037(8)

a simple localized picture where only Co^{4+} ions carry the spin moment S=1/2, the effective moments for the 0.92, 0.75, and 0.6 compositions are expected to be $0.49\mu_B$, $0.87\mu_B$, and $1.09\mu_B$ per formula unit, respectively. The observed moments are $0.32\mu_B$, $0.88\mu_B$, and $0.82\mu_B$ per formula unit, respectively. Although the differences between the calculated values assuming a simple model and the observed ones are not large, developing experiments in the two-layer phase indicate that a more complex electronic and magnetic system is at play (see, e.g., Ref. 16). It can be inferred, however, that low-spin configurations for Co^{3+} and Co^{4+} ions are found in these phases. Small deviations from the Curie law are noted for $x=0.92$ and 0.6 below 30 K, and a magnetic transition at ~30 K is seen for $x=0.75$, at a similar temperature to that observed for the two-layer $x=0.75$ phase.[16] For $x=0.5$, χ vs T has a different shape and no Curie-Weiss behavior is found. Two cusps are observed in the χ vs T data: one at ~88 K and another one at ~52 K. These two transitions are observed at nearly the same temperatures where transitions are observed for two-layer $Na_{0.5}CoO_2$.[5] In the two-layer structure the two anomalies signal the onset of an insulating state that has been attributed to a charge ordered phase. For $x=0.3$ in the three-layer structure, χ is independent of temperature above 75 K. A Curie contribution is seen at lower temperatures. The origin of this behavior is not known.

C. Resistivity measurements

Resistivity measurements were performed on $x=0.5$ single crystals (Fig. 6). A transition to an insulating state is observed. The primary resistive transition is observed at 50 K, but the derivative of the resistivity data (inset, Fig. 6) shows that the transition observed in the susceptibility near 88 K also impacts the resistivity. The behavior of the resistivity in the three-layer derived phase is very similar to that of two-layer $Na_{0.5}CoO_2$, though in the latter case the resistive transition often shows an initial increase near 50 K with the main transition at lower temperatures.

D. Heat capacity

The heat capacity data as a function of x for the three-layer derived Na_xCoO_2 phases are presented in Fig. 7. The specific heat for all compositions decreases as the temperature approaches 2 K. For $x=0.75$, a small transition is seen around 25 K, associated with the magnetic ordering observed in the χ vs T data. The electronic contribution to the specific heat (γ) was extracted from the Debye formula at

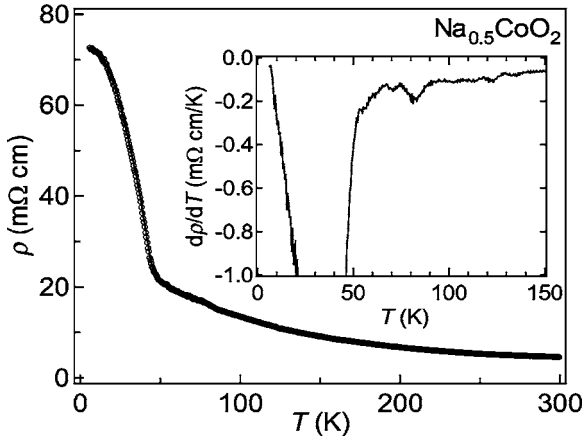

FIG. 6. The temperature dependence of the resistivity in the plane parallel to the CoO_2 layers in a single crystal of $P1$-type $Na_{0.5}CoO_2$. The inset shows the derivative curve.

temperatures lower than 10 K. The inset of the figure shows γ for each composition. As expected, the lowest γ is found for $x=0.5$ where a transition from metalic to insulator takes place. Below and above this composition, the larger carrier concentrations are expected to result in larger values for γ.

IV. DISCUSSION

In contrast to the relatively straightforward structural behavior of the frequently studied two-layer Na_xCoO_2 system, significant structural changes take place when the sodium composition is varied in three-layer derived Na_xCoO_2. In the two-layer system, $P2$-type phases exist over a large composition range, dominating the phase diagram from $x=0.3$ to 1. In that two-layer system, $x=0.5$ is a special composition structurally, and there are small two-phase regions between different $P2$-type structures in the high-sodium-content region. The Na is in trigonal prismatic coordination across the whole two-layer series, resulting in the fact that neighboring

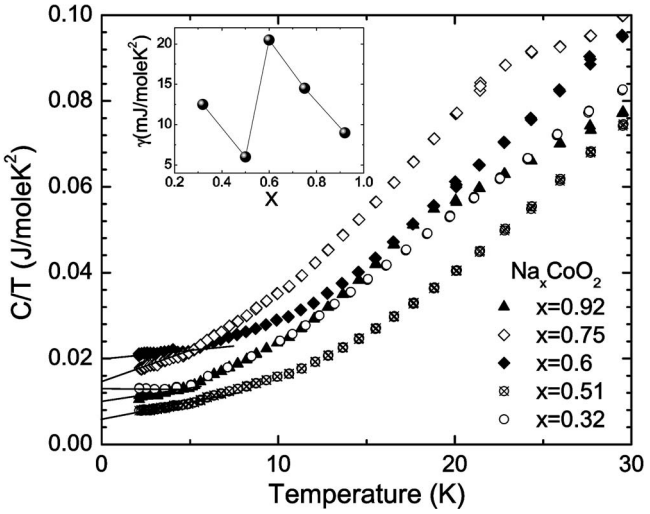

FIG. 7. Temperature dependence of the specific heat for three-layer derived Na_xCoO_2 with $x=0.92$, 0.75, 0.6, 0.51, and 0.32.

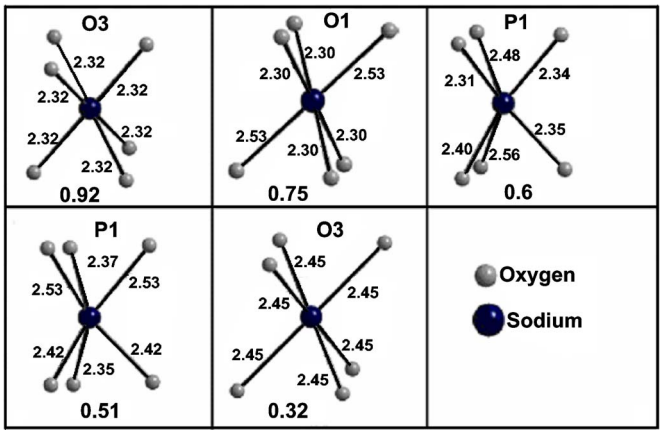

FIG. 8. (Color online) The NaO_6 coordination polyhedra found in the three-layer derived Na_xCoO_2 structures.

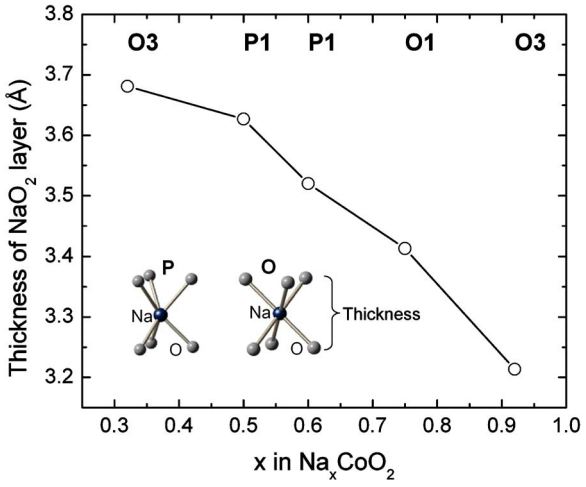

FIG. 9. (Color online) The thickness of the NaO_2 layer as a function of x in three-layer derived Na_xCoO_2.

CoO_2 layers are stacked in the same position relative to each other in all compounds. The same is not the case for the three-layer derived family. Our studies show that octahedral coordination for Na is apparently destabilized near half filling (i.e., $x \sim 0.5$) of the Na planes. The energetic reason for this is not known. The appearance of $P1$ phases in the middle of the three-layer derived phase diagram due to this octahedral site destabilization is the major factor in complicating the structural phase diagram. Thus, unlike the two-layer system, the regions of solid solution in the three-layer Na_xCoO_2 are relatively narrow and compositions intermediate to those described here are classic two-phase mixtures.

The changes in Na coordination across the series cause the CoO_2 layers to shift relative to each other to create the appropriate shape coordination polyhedra for Na and the right position of the adjacent O layers. The Na coordination polyhedra observed are presented in Fig. 8. Both the bond lengths and shapes of the octahedra and trigonal prisms are consistent with expectations for Na–O polyhedra and very similar to what is seen in the two-layer series.[7] As in the two-layer series, the NaO_2 plane layer expands as Na is removed: when the sodium site occupancy within the layers decreases, the repulsion between the CoO_2 sheets is enhanced, and also the Coulombic forces holding the layers together decrease. Figure 9 shows that in spite of the changes in coordination of the Na across the series, the thickness of the NaO_2 layers changes continuously with Na content.

A characterization of the relation of the CoO_2 planes relative to one another across the series is presented in Fig. 10. In the top panel, the distances between the CoO_2 planes (from Co plane to Co plane) are shown for all studied compounds. There is a uniform change to smaller separation with increasing Na concentration, due primarily to the changing concentration of Na in the NaO_2 plane, as described above.

The structures change symmetry across the series and the Na coordination changes from octahedral to trigonal prismatic and back again. A uniform description of the family can be made, however, by defining a pseudomonoclinic cell for all cases, with $a=a_{\mathrm{hex}}$ and $b=a_{\mathrm{hex}}\sqrt{3}$ for the in-plane cell parameters, and c the distance from one Co to its equivalent Co one layer away. The pseudomonoclinic β angle gives the angle between the c and a pseudomonoclinic axes, and is a good measure of the relative positions of neighboring layers. As an example, Fig. 11 shows the pseudomonoclinic cell derived from the hexagonal cell for x=0.92 and 0.75.

To characterize how the planes shift relative to one another across the series, the pseudomonoclinc angle and the actual distance of the plane shift on going from one compound to the next are shown in the bottom two panels of Fig. 10. The middle panel suggests that the $x=0.75$ compound has an unexpectedly large shift of the layers relative to the

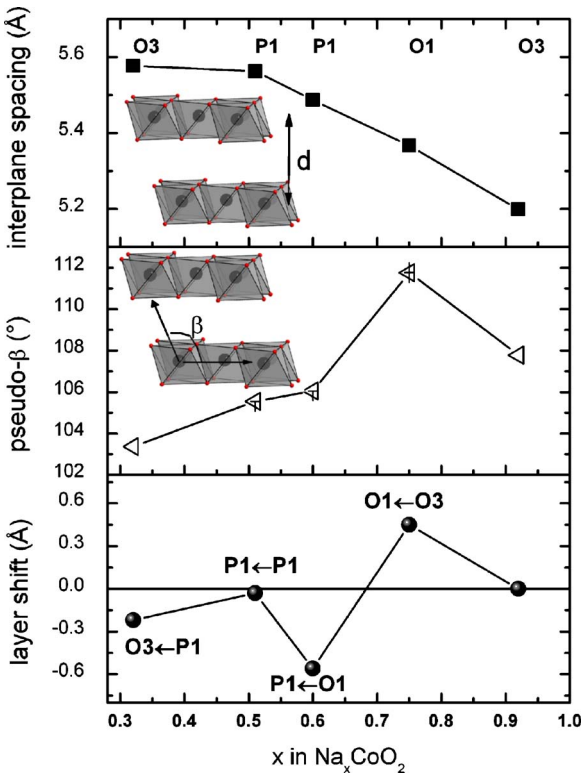

FIG. 10. (Color online) (Top) The distance between neighboring CoO_2 layers (from Co plane to Co plane); (middle) pseudomonoclinic cell angle; and (bottom) layer shift in Na_xCoO_2 phases as functions of x in three-layer derived Na_xCoO_2.

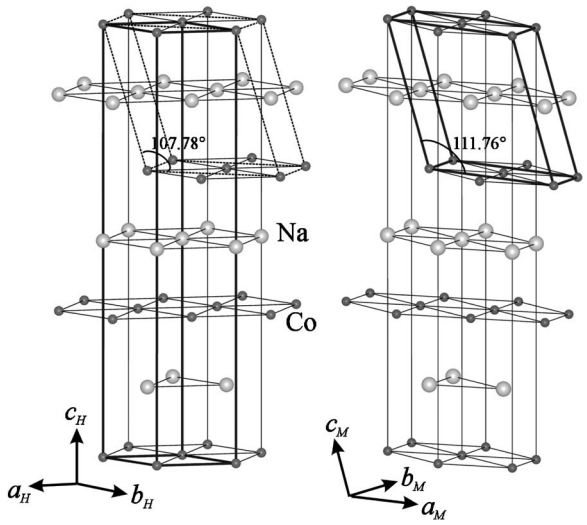

FIG. 11. The pseudomonoclinic cell derived from the three-layer hexagonal structure for x=0.92 and 0.75. The actual unit cell for both compositions is shown with thick lines.

behavior of the rest of the series, where the angles change continuously with Na concentration. This unusual character for the $x=0.75$ phase is also suggested by the bottom panel: though the coordination of the Na remains octahedral when decreasing the Na content from $x=0.92$ to 0.75, the layer has shifted by 0.6 Å. Interestingly, this shift is of the same magnitude, though in the opposite sense, as occurs when the layers shift between $x=0.75$ and 0.6 to accommodate a change in the Na coordination from octahedral to prismatic. A somewhat smaller shift is observed on going from the trigonal prismatic to octahedral coordination between x =0.51 and 0.32. It is interesting that in all cases the magnitudes of the shifts are relatively small, 0.6 Å in the largest case.

As sodium content is varied in Na_xCoO_2, the formal oxidation state of Co must change. For ideal $NaCoO_2$, $Na_{0.5}CoO_2$ and CoO_2, for example, the Co formal oxidation states will be +3, +3.5, and +4, respectively. Thus, as in the copper oxide superconductors where the charge in the CuO_2 planes can be deduced from the oxygen content or electropositive nontransition metal ratios (e.g., in $La_{2-x}Ba_xCuO_4$), the sodium content can be used as a measure of the charge state of the electronic system in the CoO_2 planes in Na_xCoO_2. There are two caveats: the strict use of Na content for this purpose in two-layer Na_xCoO_2 has been called into question for compositions where x is less than 0.5 by titration measurements,[17] and, second, as in other highly oxidized transition metal compounds, the formal charge value says nothing about how the excess positive charge, on going from Co^{3+} to Co^{4+}, is distributed among the Co or its coordinating oxygens. Plotting of structural parameters relevant to the electronic system as a function of Na content is straightforward, however, and can be used to infer general characteristics of the electronic system.

The structural characterization of the CoO_2 plane as a function of Na content in three-layer derived Na_xCoO_2 is presented in Fig. 12. As the sodium composition decreases, the in-plane Co-Co distance decreases, as seen in the top

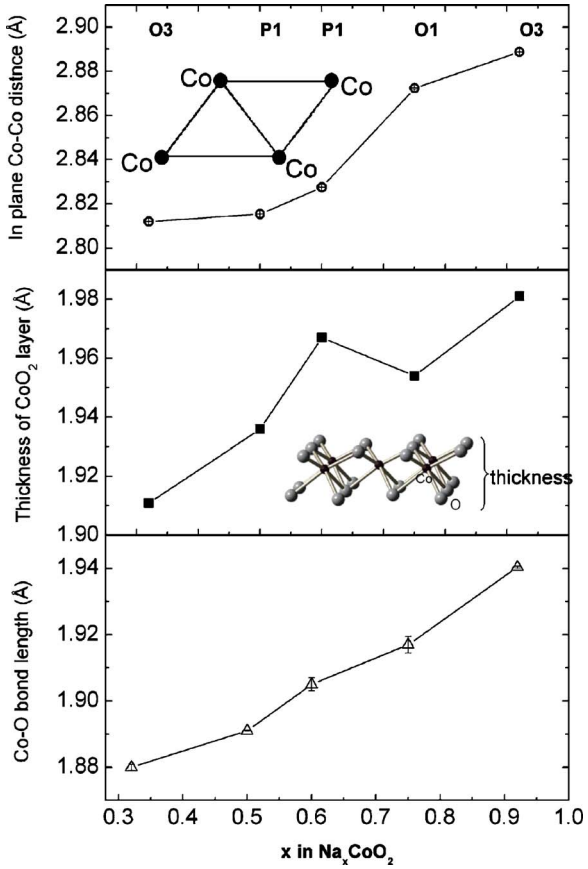

FIG. 12. (Color online) (Top) The in-plane Co-Co separation; (middle) the thickness of the CoO_2 layers; and (bottom) variation of the Co-O bond length as functions of x in three-layer derived Na_xCoO_2.

panel. In the simplest picture, this is a result of increasing the formal oxidation state of cobalt from mainly Co^{3+} in $Na_{0.92}CoO_2$ to $Co^{3.68+}$ in $Na_{0.32}CoO_2$: the in-plane size of the CoO_6 octahedra is expected to shrink as the Co^{4+} to Co^{3+} ratio increases. It is of interest that the size change, though monotonic, is not linear across the series, but changes most in the mid-composition regions. Structural study of the two-layer Na_xCoO_2 system has led to the suggestion that the thickness of the CoO_2 layers may be a good reflection of redistribution of charge among different electronic orbitals with variation of electron count in that system.[7] The thickness of the CoO_2 layer as a function of sodium content in the three-layer derived system is shown in the middle panel of Fig. 12. As expected, for $x=0.92$ where the cobalt ions are mainly Co^{3+}, the CoO_2 layer thickness is largest, because the octahedra are largest, while for $x=0.32$, where the formal oxidation state is $Co^{3.68+}$, the CoO_2 layer thickness is smallest. The figure shows (middle panel), however, that the variation in layer thickness, in this series is not monotonic, suggesting that there is a significant redistribution of charge among different electronic orbitals across the three-layer derived series as a function of Na content. Significantly, the Co-O bond length varies continuously across the series, reflecting a systematic, continuous change in the formal Co oxidation state. The data presented in this figure suggest that in three-layer derived Na_xCoO_2, the electronic system

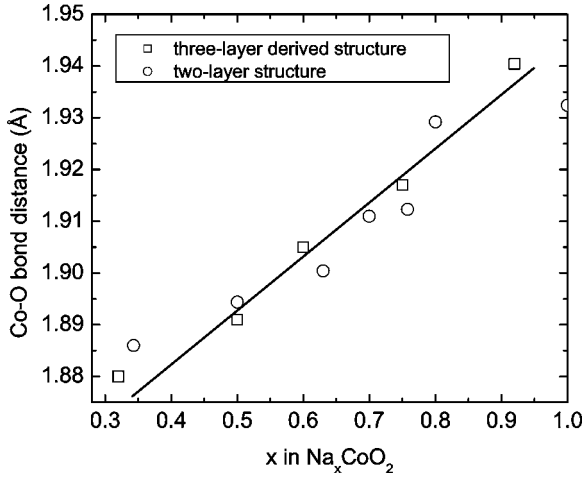

FIG. 13. Comparison of the Co-O bond lengths as a function of x in Na_xCoO_2 in the two-layer and three-layer derived series. The line drawn is a guide to the eye.

changes, and the crystal structure responds, over the whole composition region, from $x=0.32$ to 0.92.

Finally, Figs. 13 and 14 and present a general comparison of the electronic characteristics of the CoO_2 planes as a function of Na concentration in the two-layer and three-layer derived systems. Figure 13 shows that the variations in Co-O bond length across the two series are very similar, and follow the expected trend toward larger size with decreased Co oxidation state. There do appear to be subtle differences observed, but more detailed study would be required to clarify them. This type of continuous bond length change with x would not be expected if oxygen vacancies occurred in significant numbers for $x<0.5$, halting the possible oxidation state of Co at an upper limit of +3.5.

Figure 14 shows the thickness of the CoO_2 layer relative to that expected if the CoO_6 octahedra have an ideal shape, as a function of composition. This quantity is determined from the length of the edges of the in-plane face of the CoO_6 octahedra and the ideal geometric relationship between the edge length and the diagonal height of an octahedron. The CoO_2 layer is highly compressed from what is expected for ideal octahedra (only 85% of the ideal value) in both phase families, suggesting that the structural distortion should be large enough to strongly influence the relative energies of different Co 3d suborbitals. This thickness varies across the series, reflecting a redistribution of charge within the CoO_2 layers as a function of composition and comparison of the two-layer and three-layer derived phases suggests that there are subtle differences in the electronic systems. In particular, the figure suggests that the three-layer derived $Na_{0.75}CoO_2$ phase has a different kind of electronic structure than is seen in the two-layer variant at the same composition. Also shown in Fig. 14 are the single-phase and multiple regions in the two families of compounds. This indicates how strongly the type of stacking influences the crystal chemistry of these systems. In addition, the figure illustrates a comparison of the Co positions in the two-layer and three-layer derived structure types. In the former, the Co planes are eclipsed while in the latter the Co planes are staggered.

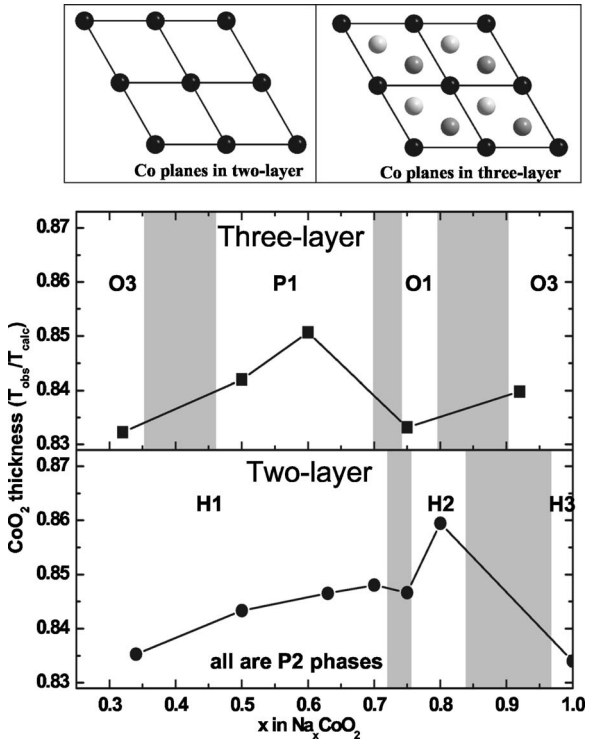

FIG. 14. Upper panel: the thickness of the CoO_2 plane relative to the thickness expected for an ideal CoO_6 octahedron (ideal thickness=1) as a function of x in three-layer derived Na_xCoO_2. Lower panel: the same characteristic for the two-layer phase. Shaded regions are two-phase regions. The nomenclature $P2$, $O3$, $O1$, and $P1$ is used to describe the Na ion coordination and the number of CoO_2 layers per cell (1, 2, or 3). $H1$, $H2$, and $H3$ refer to subtle differences in crystal structure within the $P2$ phase. The illustration on the top shows a comparison of the Co positions in the two-layer and three-layer variants. In the two-layer phases the Co planes are the same in all layers. In the three-layer derived phases the triangular Co planes are staggered: black balls represent layer 1, dark gray balls represent layer 2, and light gray balls represent layer 3.

V. CONCLUSIONS

The crystal structures of the Na_xCoO_2 phases derived from three-layer $NaCoO_2$ are more complex than the much studied two-layer structures. This is due in large part to the fact that unlike the two-layer system, in the three-layer derived system the Na coordination changes in the structural series. In the two-layer family, the sodium forms many ordered phases, both commensurate and incommensurate with the underlying CoO_2 lattice. In the present system, due to the different types of sites encountered (i.e., octahedral rather than prismatic) the Na ordering may be expected to be different. No information on that ordering is provided in the average structure determinations presented here, and would be of interest in future studies. The structural complexity of the system is reflected in the crystal structure of the $x=0.75$ composition, where unlike the case of the analogous two-layer variant, the high intensities of the incommensurate superlattice reflections suggest that the underlying CoO_2 lattice experiences some kind of structural modulation. The de-

termination of this structure will be of interest, as well as modeling to determine whether the structural modulation is electronically driven.

Magnetic susceptibility data in the current family are consistent with Co^{3+} and Co^{4+} ions being in low-spin configuration, and the magnetic behavior is similar to that observed in the two-layer system, though some differences are seen, particularly the presence of a Curie-Weiss susceptibility in the $x=0.3$ sample. The three-layer derived $x=0.5$ phase, in its initial characterization reported here, appears to be analogous to the two-layer variant, suggesting that the electronic instability that gives rise to the insulating behavior is strongly two dimensional in character, due to the fact that the stacking of the CoO_2 layers differs in the two systems. Finally, the composition dependence of the electronic contribution to the specific heat in the three-layer system appears to be substantially different from what has been reported in the two-layer system,[18–20] in the present case showing the largest γ value at $x=0.6$. This may be due to the special character of the $x=0.75$ composition in the three-layer system, which may suppress γ. These similarities and differences suggest that further work on the three-layer derived phases and comparison to the two-layer phases will be of interest.

ACKNOWLEDGMENTS

The work at Princeton was supported by the Department of Energy, Grant No. DOE-FG98-0244254, and by the National Science Foundation, Grant No. DMR-0213706.

[1] M. G. S. R. Thomas, P. G. Bruce, and J. B. Goodenough, Solid State Ionics **17**, 13 (1985).
[2] K. Takada, H. Sakurai, E. Takayama-Muromachi, F. Izumi, R. A. Dilanian, and T. Sasaki, Nature (London) **422**, 53 (2003).
[3] I. Terasaki, Y. Sasago, and K. Uchinokura, Phys. Rev. B **56**, R12685 (1997).
[4] Y. Wang, N. S. Rogado, R. J. Cava, and N. P. Ong, Nature (London) **423**, 425 (2003).
[5] M. L. Foo, Y. Wang, S. Watauchi, H. W. Zandbergen, T. He, R. J. Cava, and N. P. Ong, Phys. Rev. Lett. **92**, 247001 (2004).
[6] Claude Fouassier, Guy Matejka, Jean-Maurice Reau, and Paul Hagenmuller, J. Solid State Chem. **6**, 532 (1973).
[7] Q. Huang, M. L. Foo, R. A. Pascal, Jr., J. W. Lynn, B. H. Toby, T. He, H. W. Zandbergen, and R. J. Cava, Phys. Rev. B **70**, 184110 (2004).
[8] Y. Takahashi, Y. Gotoh, and J. Akimoto, J. Solid State Chem. **172**, 22 (2003).
[9] Y. Ono, R. Ishikawa, Y. Miyazaki, Y. Ishii, Y. Morii, and T. Kajitani, J. Solid State Chem. **166**, 177 (2002).
[10] S. Kikkawa, S. Miyazaki, and M. Koizumi, J. Solid State Chem. **62**, 35 (1986).
[11] A. Larson and R. B. Von Dreele, Computer code GSAS, Los Alamos National Laboratory, Los Alamos, NM, 1994.
[12] Certain commercial products or equipment are identified in this paper to describe the subject adequately. Such identification does not imply recommendation or endorsement by the NIST, nor does it imply that the equipment identified is necessarily the best available for the purpose.
[13] C. Delmas, J. J. Braconnier, C. Fouassier, and P. Hagenmuller, Solid State Ionics **3/4**, 165 (1981).
[14] Q. Huang, M. L. Foo, J. W. Lynn, H. W. Zandbergen, G. Lawes, Y. Wang, B. H. Toby, A. P. Ramirez, N. P. Ong, and R. J. Cava, J. Phys.: Condens. Matter **16**, 5803 (2004).
[15] A. J. Williams, J. P. Attfield, M. L. Foo, L. Viciu, and R. J. Cava, Phys. Rev. B (to be published).
[16] J. L. Gavilano, D. Rau, B. Pedrini, J. Hinderer, H. R. Ott, S. M. Kazakov, and J. Karpinski, Phys. Rev. B **69**, 100404(R) (2004).
[17] M. Karppinen, I. Asako, T. Motohashi, and H. Yamauchi, Phys. Rev. B **71**, 092105 (2005).
[18] M. Yokoi, T. Moyoshi, Y. Kobayashi, M. Soda, Y. Yasui, M. Sato, and K. Kakumai, J. Phys. Soc. Jpn. **74**, 3046 (2005).
[19] R. Jin, B. C. Sales, S. Li, and D. Mandrus, Phys. Rev. B **72**, 060512(R) (2005).
[20] M. Brühwiler, B. Batlogg, S. M. Kazakov, and J. Karpinski, cond-mat/0309311 (unpublished).